JOURNAL OF THERMOPHYSICS AND HEAT TRANSFER
Vol. 22, No. 3, July–September 2008

Visual Observation of Oscillating Heat Pipes Using Neutron Radiography

C. Wilson,* B. Borgmeyer,* R. A. Winholtz,† and H. B. Ma‡
University of Missouri—Columbia, Columbia, Missouri 65211
and
D. L. Jacobson,§ D. S. Hussey,§ and M. Arif§
National Institute of Standards and Technology, Gaithersburg, Maryland 20899

DOI: 10.2514/1.33758

Qualitative observation of flow patterns in water and nanofluid oscillating heat pipes was conducted at various heat inputs and condenser temperatures. Images of the liquid flow within the copper tubing were first captured at 30 frames per second using neutron radiography. Neutron radiography allows direct observation of a fluid position because liquid water is hydrogen rich and opaque while water vapor (because it is much less dense) and the other materials in the oscillating heat pipes are transparent. Flow visualization was conducted on an 8-turn water oscillating heat pipe, an 8-turn nanofluid oscillating heat pipe, and a 12-turn nanofluid oscillating heat pipe. The water oscillating heat pipe was filled with high performance liquid chromatography grade water. The 12-turn nanofluid oscillating heat pipe was filled with 1% by volume ($35.0\ \mathrm{g \cdot ml^{-1}}$) diamond nanoparticles in high performance liquid chromatography water and the 8-turn oscillating heat pipe contained 0.016% by volume ($0.5\ \mathrm{mg \cdot ml^{-1}}$) diamond nanoparticles high performance liquid chromatography water. The diamond nanoparticles were 5 to 50 nm in diameter. All oscillating heat pipes were charged at a filling ratio of 50%. Visual observation shows for all heat pipes that at low heat inputs, fluid oscillation is very random and intermittent. Increasing the heat input causes a steady flow pattern to appear. For all tested oscillating heat pipes, increased heat load or operating temperature resulted in an increased fluid velocity. Also, nucleation was never observed in the tested oscillating heat pipes.

Introduction

OSCILLATING heat pipes (OHP) transport heat via a multiphase fluid in a small diameter tube that crosses evaporator and condenser regions. For the OHP to work, this tube diameter must be small enough to form liquid plugs and vapor slugs, and prevent liquid and vapor counterflow. The maximum tube diameter can be calculated by the Bond number, $Bo = (\rho_l - \rho_v)gD^2/4\sigma$ [1], where σ is the surface tension, g is the gravitational acceleration, ρ_l is the liquid density, D is the inside diameter of the tube, and ρ_v is the vapor density. When the surface tension is higher than the gravitational force, that is, $Bo < 1.0$, the liquid plugs and vapor slugs can be formed in the tube. By using the temperature difference and therefore a pressure gradient between the evaporator and condenser, the fluid and vapor are forced to oscillate between these two regions, transferring heat. Generally by increasing the number of times the tube crosses the evaporator and condenser, the performance increases. A turn is defined as a tube passing from the evaporator, turning in the condenser, and returning to the evaporator. Because the fluid flow of liquid plugs and vapor slugs plays a key role in the heat transfer enhancement in the OHP, the flow behavior is very important. Several experiments have been conducted where the OHP was built out of glass or plastic for visual observation of the fluid movement [2–7]. Because the low thermal conductivities of glass or plastic materials, the fluid flow and heat transfer behaviors are different from OHPs constructed of the original materials such as the copper tubing.

Nanofluid OHPs demonstrated in earlier research [8,9] have higher heat transport capabilities than their water counterparts. One reason might be due to the increased thermal conductivity which has been generally observed in nanofluids [10–12]. The current investigation is to use neutron radiography to directly visualize fluid motion in OHPs constructed out of copper material. Three OHPs were tested in these experiments. One of these contained water and two contained diamond nanofluid, all with a filling ratio of 50%.

Experimental Setup

The experiment was performed at the National Institute of Standards and Technology (NIST) research reactor in Gaithersburg, Maryland. Using the thermal neutron imaging experimental facility at NIST [13], we were able to record neutron images at a video rate allowing visualization of the fluid movement within the copper OHPs. Neutron radiography uses a beam of neutrons that pass through the imaged object and strike a detector. When the neutrons pass through the object, they are scattered and absorbed by the elements within it. Different elements and density of materials result in varying amounts of neutron attenuation. The thickness for a $1/e$ drop in intensity is given by the Lambert–Beer law of attenuation

$$t_{1/e} = \frac{1}{\sum_i N_A \rho (\sigma_i / A_i) w_i}$$

where i refers to an isotope, σ_i is the total scattering cross section, ρ is the mass density, A_i is the atomic weight, and w_i is the weight fraction. The $1/e$ thicknesses for materials in the beam path are shown in Table 1. Neutron radiography shows the fluid motion within the OHP, because the neutron attenuation of the hydrogen component of water is much higher than that of the metals and nanoparticles used in the OHP. In addition, the density difference between the liquid and vapor phases is easily detectable in the resulting images. Therefore, in the images, liquid water blocks most neutrons from reaching the detector, while water vapor, diamond nanoparticles, copper, and aluminum are significantly more transparent.

Received 30 July 2007; revision received 24 November 2007; accepted for publication 10 December 2007.

*Ph.D. Student, Department of Mechanical and Aerospace Engineering.
†Associate Professor, Department of Mechanical and Arospace Engineering.
‡LaPierre Associate Professor, Department of Mechanical and Aerospace Engineering; mah@missouri.edu (Corresponding Author).
§Physicist, Physics Laboratory.

Table 1 Thickness of material for a $1/e$ drop in thermal neutron beam intensity [14]

Material	$t_{1/e}$, cm
Water–liquid	0.286
Water–vapor	11140
Carbon–diamond	1.02
Copper	1.41
Aluminum	11.0
Silica insulation (approximate density 0.02 g · cm^{-3})	462

Figure 1 shows the setup of the experiments. The OHP was placed between the camera and the beam port on an adjustable test stand. Neutron masks were positioned in front of the OHP to prevent unnecessary irradiation. The remainder of the equipment was placed outside the neutron imaging hutch. Power was supplied to the OHP heater via a Staco 3PN1010B power supply and measured with a digital multimeter (DMM). The OHP was cooled via a Julabo F34/MD circulator. Temperatures were acquired with computer 1 using a National Instruments SCXI 1600 data acquisition card (DAQ). Computer 2 acquired 12-bit images at 30 fps. The temperature sample rate varied from 50–250 Hz depending on the length of the test. At the beginning of each test the image acquisition software in computer 2 triggered the temperature DAQ so that the temperature data and images would be synchronized. Because of the light water cooled design of the OHP, the cooling water blocked any visual observation of the OHP in the condensing region. To reduce irradiation of the cooling water and unnecessary irradiation of the OHP, the mask was adjusted to block this region from the neutrons.

Three OHPs were tested with this setup. These include a 12-turn nanofluid OHP (Fig. 2), an 8-turn water OHP (Fig. 3), and an 8-turn nanofluid OHP (Fig. 3). All OHPs had a fill ratio of 50% and used high performance liquid chromatography (HPLC) grade water. The OHPs were charged by first degassing the empty OHP and the charging fluid with a vacuum pump. Then the OHP was backfilled and excess fluid was removed. The 12-turn OHP nanofluid contained water and 1% by volume (35.0 mg · ml^{-1}) diamond nanoparticles. The 8-turn OHP contained 0.016% by volume (0.5 mg · ml^{-1}) diamond nanoparticles.

The dimensions of the OHPs are shown in Figs. 2 and 3. The construction of the 8- and 12-turn OHPs is very similar. Two 0.635-cm (0.25-in.) thick copper plates spread heat from the copper tubing to the condensing blocks and the heater. To provide a large contact area between the plates and the 0.32-cm (0.125-in.) copper tubing, 0.32-cm (0.125-in.) semicircular grooves were machined into the plates. Omegabond "201" [15] thermal paste was placed between the groove and the tube to reduce the contact resistance.

These OHPs were positioned vertically with the evaporator below the condenser. They were insulated with aluminum foil encased fiberglass insulation (which is assumed to have a similar neutron transmission to silica). The aluminum foil prevented any of the fiberglass from becoming airborne. Several adjustments were made to the video images: the images were dark field and bright field corrected, and the scale was adjusted for contrast to give definition between the fluid and vapor regions.

Results and Discussion

Figure 4 illustrates the transient process of the 12-turn OHP after a power input of 300 W was added on the evaporating section of the OHP. The transient operation of the OHP has several stages. In stage 1 after heat is added to the evaporator, the vapor expands within the evaporator slowly pushing the liquid toward the condenser (Fig. 5: $t = 0, 5, 10$ s). During stage 2, starting at about 15 s, some liquid and vapor portions in the condenser also began to slowly and smoothly move toward the evaporator region (Fig. 4: $t = 15, 25, 35, 45$ s). Stage 3 begins around 50 s and is characterized by some very slow flow reversals (Fig. 4: $t = 50, 55, 60$ s s). At 1 min, stage 4, there is a sudden transition to persistent rapid oscillating behavior (Fig. 4: $t = 60, 65, 70, 75$ s). This oscillation motion occurs very quickly and appears to occur throughout the heat pipe. During all of these regions,

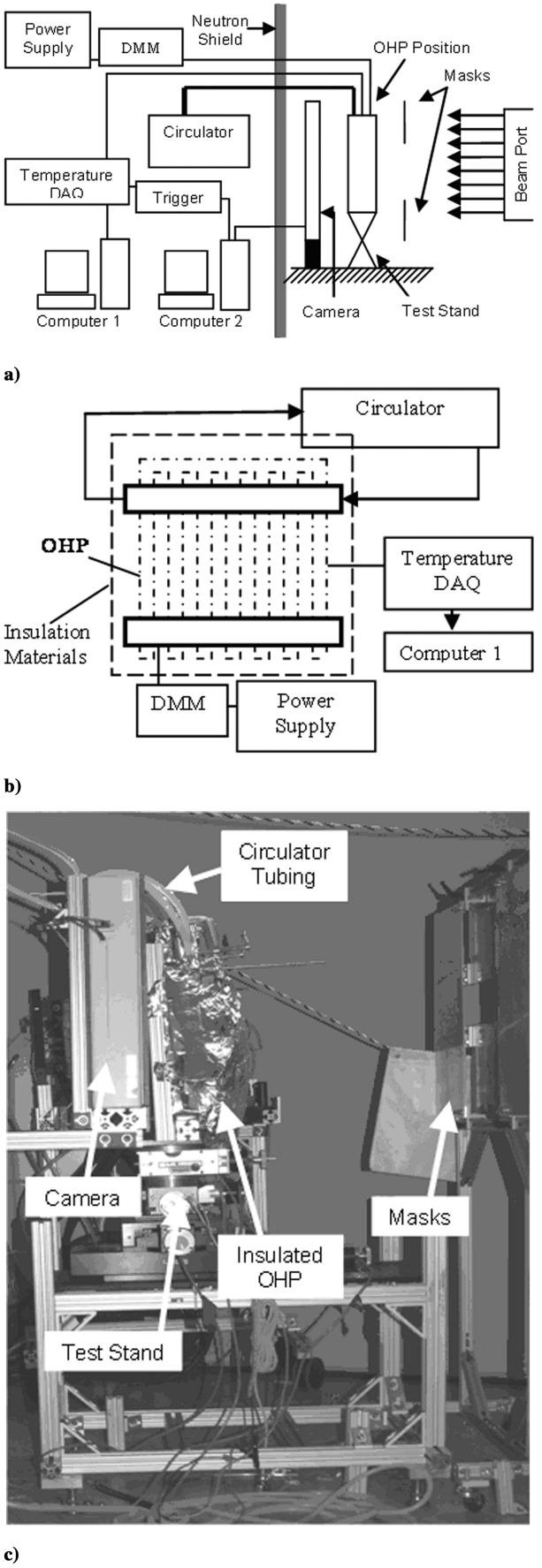

Fig. 1 Experimental systems: a) entire experimental setup, b) experimental setup for OHP, and c) picture of experimental setup.

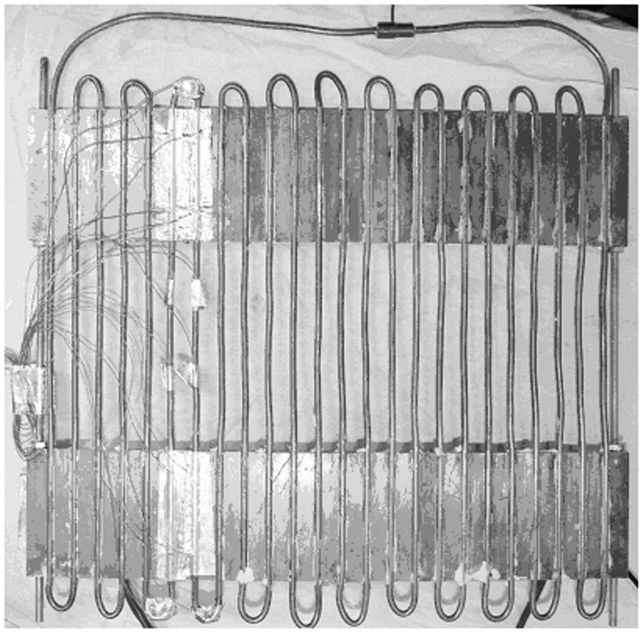

a)

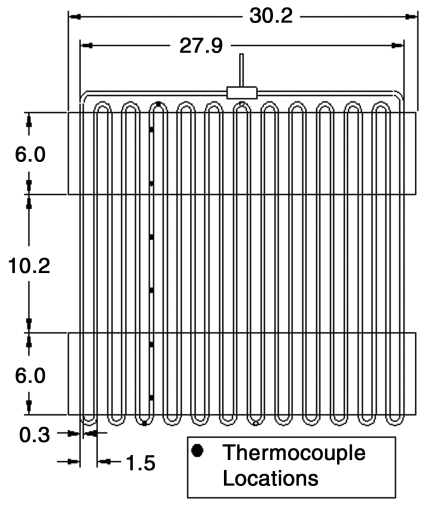

b)

Fig. 2 12-turn oscillating heat pipe: a) photo; b) dimensions (units in cm).

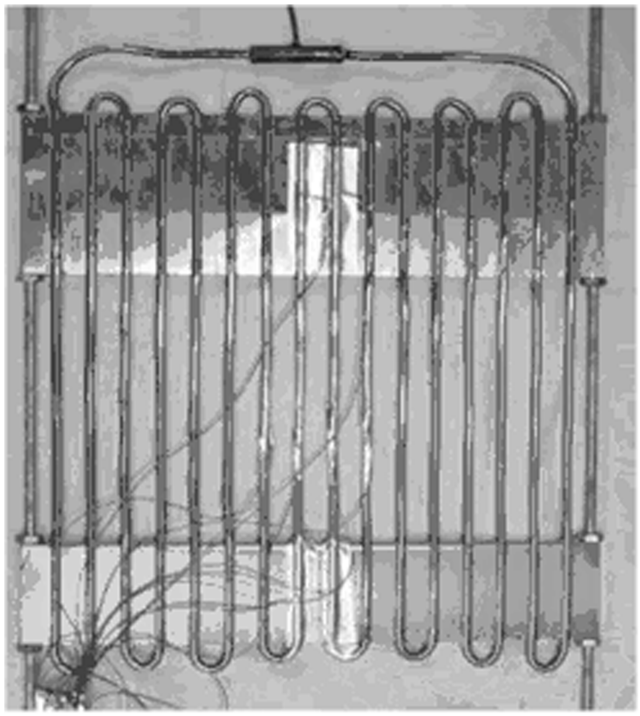

a)

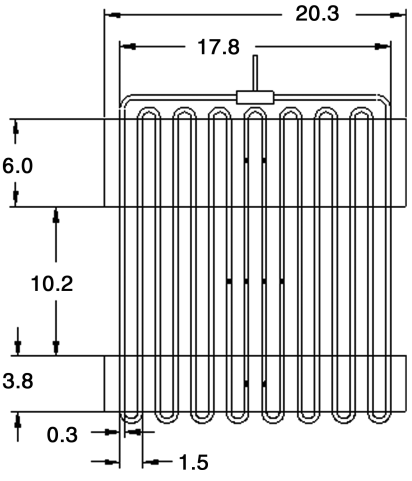

b)

Fig. 3 8-turn oscillating heat pipe: a) photo; b) dimensions (units in cm).

the temperature response is very smooth and the fluid oscillations are barely noticeable in the temperature measurements. Note that the temperature oscillations do not begin until 125 s, well after significant fluid movements were observed.

The flow characteristics of the different OHPs were very similar. They were characterized by fast fluid movement at the center turns of the OHP as shown in Fig. 6, with very little movement in the outer turns, and almost no bulk flow. (The motion of the fluid was derived from all frames, not just the ones presented in this text.) This is also illustrated in Fig. 6 with the 8-turn nanofluid OHP at 199.5 W. This flow distribution in the 8- and 12-turn OHPs was likely due to a nonuniform heat flux provided by the strip heater. The outer turns of the OHP received a lower heat flux while the inner turns received a higher heat flux. Besides the nonuniform movement of the OHP, each OHP exhibited slightly different flow patterns. At the same heat load and operating temperature, each heat pipe behaved slightly differently. The 12-turn nanofluid OHP had the lowest frequency and amplitude temperature oscillations. The heat flux per tube of the 12-turn OHP was lower than the 8-turn OHP, which should be one of the reasons for a lower frequency and amplitude. Also, the 8-turn nanofluid OHP had a lower frequency

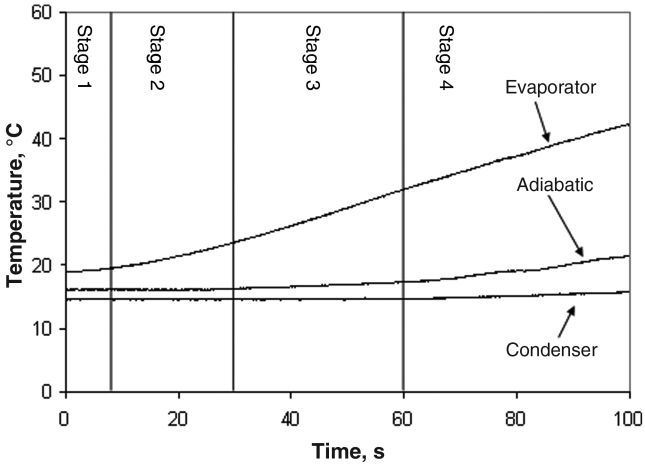

Fig. 4 Transient process of a 12-turn OHP ($W = 300.0$ W, filling ratio = 50%).

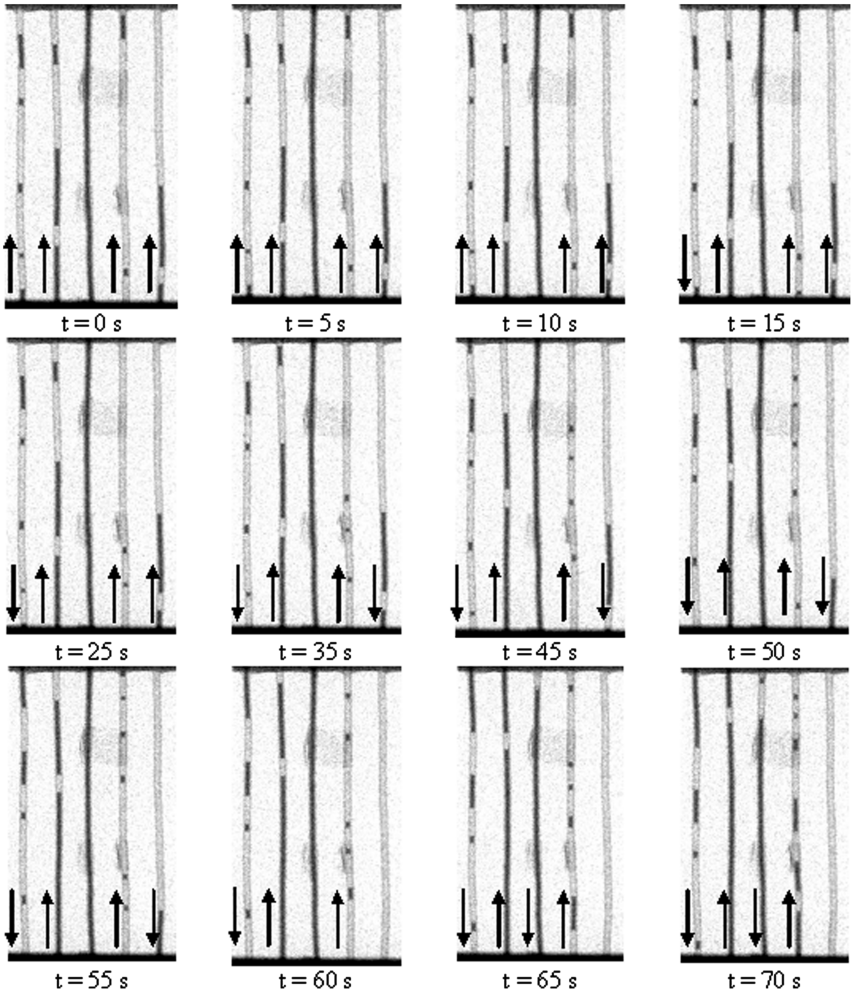

Fig. 5 Fluid distribution with time for the 12-turn OHP with a 300-W step input at $t = 0$ s.

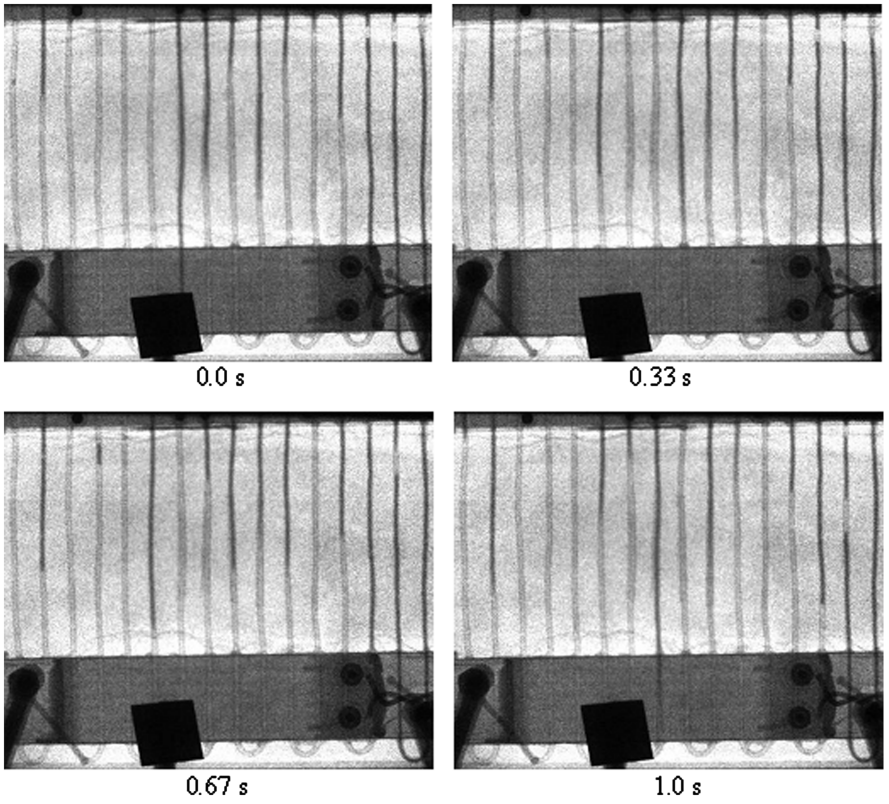

Fig. 6 Nonuniform flow in the 8-turn nanofluid OHP at 199.5 W.

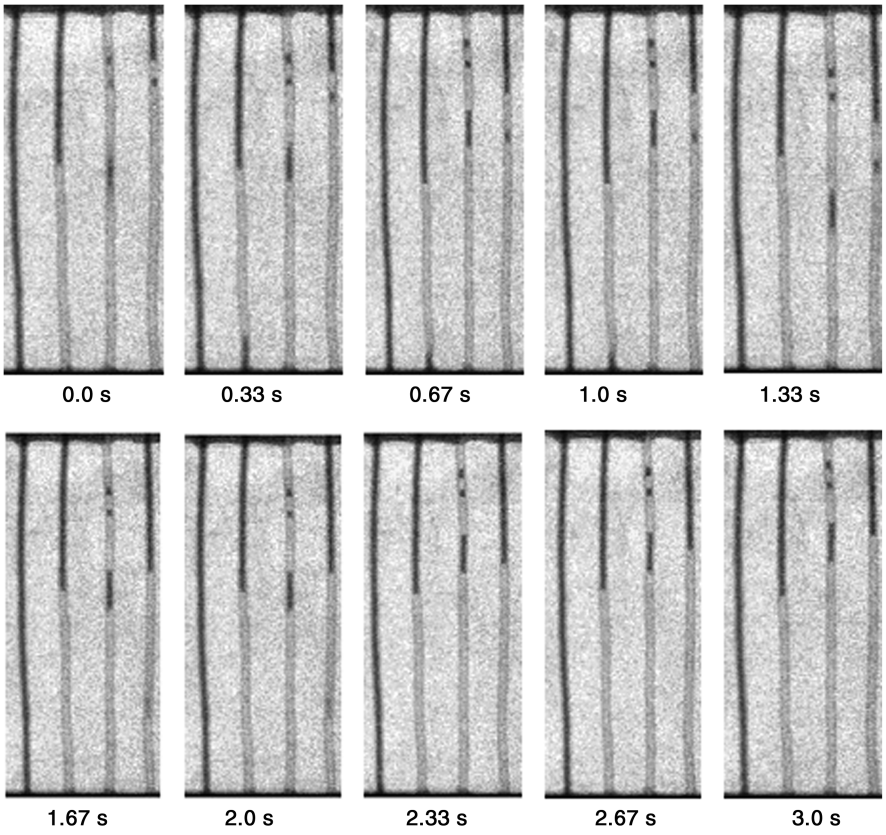

Fig. 7 Fluid movement in the center turns of the 12-turn nanofluid OHP at 50.5 W and an operating temperature of 20°C.

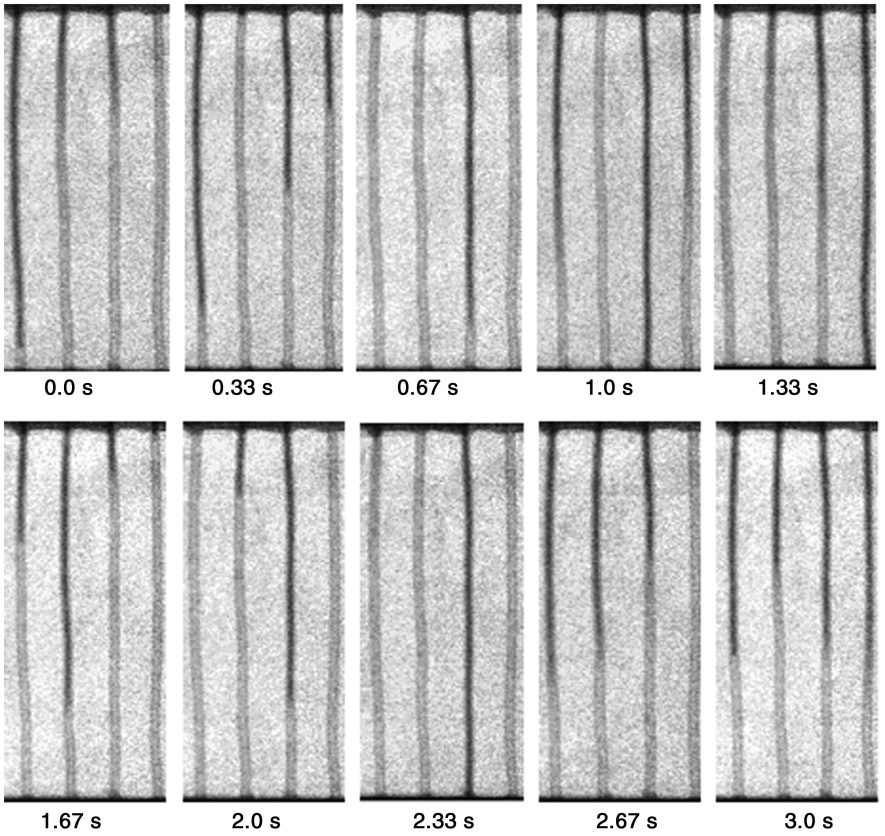

Fig. 8 Fluid movement in the center turns of the 12-turn nanofluid OHP at 199.4 W and an operating temperature of 20°C.

and amplitude than the 8-turn water OHP. The high thermal conductivity of the nanofluid OHP can transfer more heat per slug of liquid and therefore allowed the OHP to transfer the same amount of heat with less movement.

Increasing the heat load of the OHP caused a noticeable increase in fluid velocity and oscillating amplitude. This is illustrated with the 12-turn nanofluid OHP at 50.5 W (Fig. 7) in which the slugs are relatively stagnant and 199.4 W (Fig. 8) in which there is a marked

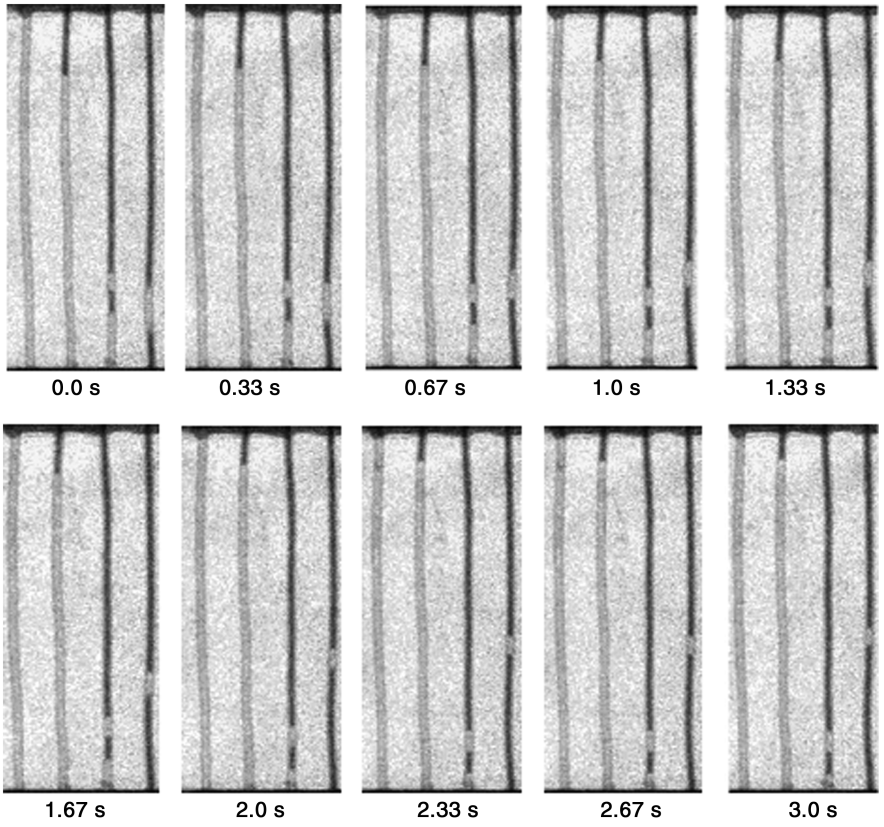

Fig. 9 Fluid movement in the center turns of the 12-turn nanofluid OHP at 50.1 W and an operating temperature of 60°C.

increase in the slug motion. For the 12-turn nanofluid OHP at 50.5 W, the bulk fluid moved very slowly with minor low amplitude fluctuations. At 199.4 W, the fluid movement was much faster. This is observable in Fig. 9 by the blurring occurring in these images and is a result of the image capture rate of 30 Hz. The blurring is the result of the fluid moving a substantial distance during the data collection time interval for the frame.

From a thermal perspective, increasing the condenser temperature significantly reduced the temperature difference between the evaporator and the condenser. Visually, the fluid motion for an operating temperature of 60°C had a slightly higher frequency and amplitude than the fluid motion at 20°C. This is shown with the 12-turn OHP at operating temperatures of 20 and 60°C in Figs. 7 and 9, respectively. However, because the fluid velocity change was not as substantial as with increased heat flux, this trend is hard to observe in these figures.

Nucleation was never observed in the middle of a liquid slug in a low level of heat input where the flow velocity was low and the vapor bubble would be easily detectable. When the heat flux level was high, the flow velocity was high; the motion blur of the liquid–vapor interface and the low resolution of the video obscure these occurrences from being observed. In addition, the condenser region was not visible; therefore it was impossible to determine if vapor bubbles were completely condensing in this region. Occasionally in the adiabatic region near the condenser, vapor was observed to condense, but vapor bubble collapse was not seen.

When the heat input level was low and the flow velocity was low, the liquid plugs and vapor bubbles can be easily detected. The images show that the liquid plug and vapor bubble pattern was not changed with time. It indirectly shows that the vapor bubbles were not collapsed; otherwise the liquid plug and vapor bubble pattern should be different with time.

Conclusions

Neutron radiography presents a unique way to observe fluid flow within OHPs. Because fluid flow and temperature are easily observable, this can lead to more accurate correlations between them. The following observations were obtained: 1) Fluid movement and oscillations started well before temperature oscillations of the OHP. 2) Increasing heat load and temperature increase the fluid velocity. 3) The oscillating motion and circulation of the liquid plug and vapor bubbles were observed. 4) Nucleation was never observed in a low level of heat input. When the heat input level was high, nucleation was not observed either, but this could be due to the temporal and spatial limitations of the neutron imaging detector. 5) Vapor bubble collapse was not observed. 6) At a given heat input, the nanofluid oscillating heat pipe produces a lower frequency and aptitude than that charged with pure water. We plan future studies aimed at obtaining more quantitative results of fluid velocity.

Acknowledgments

The work presented in this paper was funded by the Office of Naval Research Grant No. N00014-06-1-1119 directed by Mark Spector, and the National Institute of Standards and Technology.

References

[1] Ma, H. B., Peterson, G. P., and Pratt, D. M., "Disjoining Pressure Effect on the Wetting Characteristics in a Capillary Tube," *Microscale Thermophysical Engineering*, Vol. 2, No. 4, 1998, pp. 283–297.

[2] Xu, J. L., Li, Y. X., and Wong, T. N., "High Speed Flow Visualization of a Closed Loop Pulsating Heat Pipe," *International Journal of Heat and Mass Transfer*, Vol. 48, No. 16, 2005, pp. 3338–3351. doi:10.1016/j.ijheatmasstransfer.2005.02.034

[3] Qu, W., and Ma, H. B., "Theoretical Analysis of Start-Up of a Pulsating Heat Pipe," *International Journal of Heat and Mass Transfer*, Vol. 50, June 2007, pp. 2309–2316. doi:10.1016/j.ijheatmasstransfer.2006.10.043

[4] Cai, Q., Chen, R., and Chen, C., "An Investigation of Evaporation, Boiling, and Heat Transport Performance in Pulsating Heat Pipe," *Proceedings of IMECE2002 ASME International Mechanical Engineering Congress & Exposition*, ASME, Fairfield, NJ, 2002, pp. 99–104.

[5] Borgmeyer, B., and Ma, H. B., "Experimental Investigation of Oscillating Motions in a Flat Plate Pulsating Heat Pipe," *Journal of*

Thermophysics and Heat Transfer, Vol. 21, No. 2, 2007, pp. 405–409. doi:10.2514/1.23263

[6] Cao, X., and Cheng, P., "A Novel Design of Pulsating Heat Pipes with Improved Performance," *13th International Heat Pipe Conference (13th IHPC)*, Shanghai Scientific & Technical Publishers, Shanghai, 21–25 Sept. 2004, pp. 302–307.

[7] Li, Y., Xu, J., and Li, Y., "Study of Pulsating Heat Pipe in GIEC, CAS," *13th International Heat Pipe Conference (13th IHPC)*, Shanghai Scientific & Technical Publishers, Shanghai, 21–25 Sept. 2004, pp. 321–328.

[8] Ma, H. B., Wilson, C., Bogmeyer, B., Park, K., Yu, Q., Tirumala, M., and Choi, S. U. S., "Nanofluid Effect on the Heat Transport Capability in an Oscillating Heat Pipe," *Applied Physics Letters*, Vol. 88, No. 14, 2006, pp. 1161–1163. doi:10.1063/1.2192971

[9] Ma, H. B., Wilson, C., Yu, Q., Park, K., Choi, S. U. S., and Tirumala, M., "An Experimental Investigation of Heat Transport Capability in a Nanofluid Oscillating Heat Pipe," *Journal of Heat Transfer*, Vol. 128, Nov. 2006, pp. 1213–1216. doi:10.1115/1.2352789

[10] Liu, M. S., Lin M. C. C., Huang, I. T., and Wang, C. C., "Enhancement of Thermal Conductivity with Carbon Nanotube for Nanofluids," *International Communications in Heat and Mass Transfer*, Vol. 32, Nov. 2005, pp. 1202–1210. doi:10.1016/j.icheatmasstransfer.2005.05.005

[11] Eastman, J. A., Choi, S. U. S., Li, S., Yu, W., and Thompson, L. J., "Anomalously Increased Effective Thermal Conductivities of Ethylene Glycol-Based Nanofluids Containing Copper Nanoparticles," *Applied Physics Letters*, Vol. 78, No. 6, 2001, pp. 718–720. doi:10.1063/1.1341218

[12] Choi, S. U. S., Zhang, Z. G., Yu, W., Lockwood, F. E., and Grulke, E. A., "Anomalous Thermal Conductivity Enhancement in Nanotube Suspensions," *Applied Physics Letters*, Vol. 79, No. 14, 2001, pp. 2252–2254. doi:10.1063/1.1408272

[13] Hussey, D. S., Jacobson, D. L., Arif, M., Huffman, P. R., Williams, R. E., and Cook, J. C., "New Neutron Imaging Facility at the NIST," *Nuclear Instruments and Methods in Physics Research, Section A*, Vol. 542, April 2005, pp. 9–15. doi:10.1016/j.nima.2005.01.004

[14] Wilson, A. J. C., *International Tables for Crystallography*, Kluwer Academic, Boston, 1992, Vol. C, pp. 384–385.

[15] Incropera, F. P., and DeWitt, D. P., *Introduction to Heat Transfer*, 4th ed., Wiley, New York, 2002.